Supplementary Material (ESI) for Chemical Communications

Three-dimensional carbon nanotube networks with supported nickel oxide nanonet for high-performance supercapacitors

Mao-Sung Wu*, Yo-Ru Zheng and Guan-Wei Lin

Department of Chemical and Materials Engineering, National Kaohsiung University of Applied Sciences, Kaohsiung 807, Taiwan

Experimental details

Graphitized multiwalled CNTs (carbon nanotubes) were purchased from ECHO Chemical Co. Ltd. (Taiwan) with an external diameter of 20–40 nm and a length of 0.5–200 μm. The raw CNT powder was etched in 15 M boiling nitric acid solution for 1h. The CNTs were then washed several times with de-ionized water until the pH value of the solution became neutral. Nickel hydroxide nanonets were grown on the bare stainless steel (SS) and SS-supported CNT film by a simple hydrothermal method. In a typical procedure, $NiSO_4 \cdot 6H_2O$ (0.09 g) and urea (0.09 g) were dissolved in deionized water (30 mL) under continuous magnetic stirring at room temperature for 30 min to form a homogenous solution. The mixture was then transferred into a Teflon-lined SS autoclave. SS sheets of type 304 (2 cm x 2 cm) were used as the electrode substrate. SS sheets were polished by emery paper with grain size of about 65 μm, and cleaned by rinsing with acetone then rinsed with de-ionized water to remove any trace of contaminants from their surface. The SS-supported CNT film was prepared by EPD (electrophoretic deposition) in a suspension containing CNT powder (20 mg), 0.1 mM $Ni(NO_3)_2$, and isopropyl alcohol (50 mL). The nickel nitrate acted as a charging agent for facilitating the dispersion and EPD of CNTs. EPD was carried out by applying a potential difference of –60 V (Keithley, 2400 source meter) across the working (negative electrode, SS) and counter (positive electrode, Pt) electrodes at room temperature. The working electrode was placed in between two parallel Pt counter electrodes. After EPD, the electrode with attached CNT film was rinsed with de-ionized water and then dried at 300°C for 1 h. The mass loading of CNT film was measured to be 0.22 mg. Two sheets of SS or SS-supported CNT film were put into the

autoclave for hydrothermal reaction. The autoclave was capped, and then heated to 95°C and held at that temperature for 6 h in an electric oven. After cooling to room temperature, the electrodes with attached nickel hydroxide products were rinsed several times with de-ionized water, and then the electrodes were annealed at 300°C for 3 h in air to convert the nickel hydroxide to nickel oxide. The amounts of active material (NiO) on the SS and CNT/SS substrates were measured to be 0.34 and 0.37 mg, respectively.

Thermal gravimetric analysis (TGA) was carried out in air at a heating rate of 10°C min^{-1} using a thermal analyzer (TA Instruments, SDT Q600). The crystal structure of nickel oxide/hydroxide samples was identified by an X-ray diffractometer (XRD, Bruker D8 Advance). The internal microstructure of samples was characterized by a transmission electron microscopy (TEM, Jeol JEM-1400). For TGA, XRD, and TEM measurements, the sample was scraped off from the SS substrate. The surface morphology of electrodes was examined with scanning electron microscopy (SEM). The specific surface area and pore size distribution of samples after heat-treated at 300 °C for 3 h was measured by the Brunauer-Emmett-Teller (BET) technique (Micromeritics, ASAP 2020) using N_2 gas adsorption/desorption. Capacitive behavior of the electrodes was determined in 1 M KOH solution by cyclic voltammetry in a homemade three-electrode cell equipped with a working electrode, counter electrode (Pt, 2 cm × 2 cm), and saturated Ag/AgCl electrode at ambient temperature. The nickel oxide electrode was used as a working electrode and placed in between two parallel Pt counter electrodes. The potential was swept linearly with time at a rate of 10 mV s^{-1} using a potentiostat (CH Instruments, CHI 608) in a potential range of 0.0-0.5 V. Galvanostatic charge and discharge tests were carried out by a source meter (Keithley, 2400) at various current densities. Electrodes were charged to a cut-off potential of 0.45 V or a cut-off capacitance of 2000 F g^{-1}, and then discharged to a cut-off potential of 0.0 V during galvanostatic charge and discharge tests. Cycle-life stability of the electrodes was investigated at a charge/discharge current density of 50 A g^{-1}. Before the electrochemical measurements, the activation of electrodes was carried out by cyclic voltammetry in 1 M KOH solution for 20 cycles at a scan rate of 25 mV s^{-1} in a potential range of 0–0.45 V. All data acquisitions using the Keithley 2400 instrument were carried out with a personal computer through the GPIB (General Purpose Interface Bus, IEEE-488) interface with LabVIEW software.

SEM images of CNT/SS, NiO/SS, and NiO/CNT electrodes

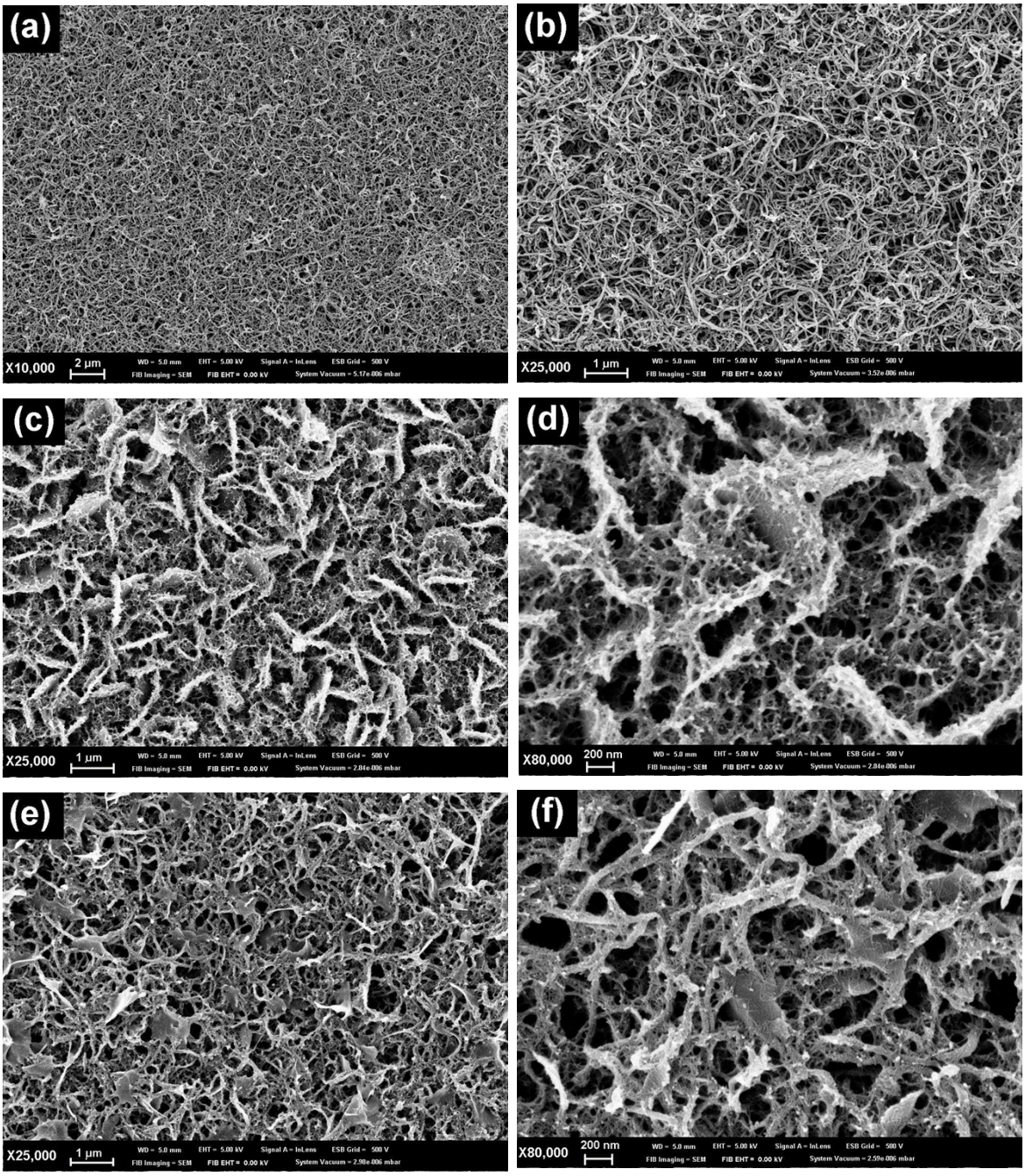

Fig. S1 SEM images of (a,b) CNT/SS, (c,d) NiO/SS, and (e,f) NiO/CNT electrodes.

TEM images of NiO nanonet and CNT film with attached NiO nanonet

Fig. S2a shows the TEM image of NiO nanonet. Sample was heated at 300°C and then scraped off from the SS substrate before TEM measurement. Clearly, the nanonet is composed of nanowires with ultrasmall diameters (< 10 nm). Fig. S2b shows the NiO nanowires grown along the large CNT. Fig. S2c shows the CNT film with attached NiO nanonet.

(a)

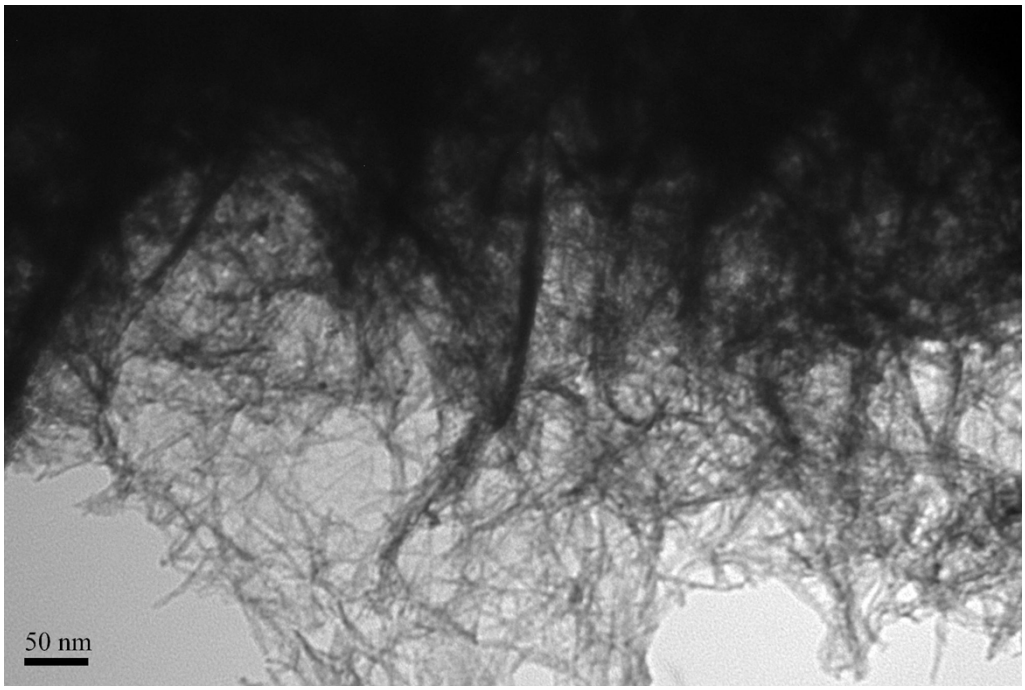

(b)

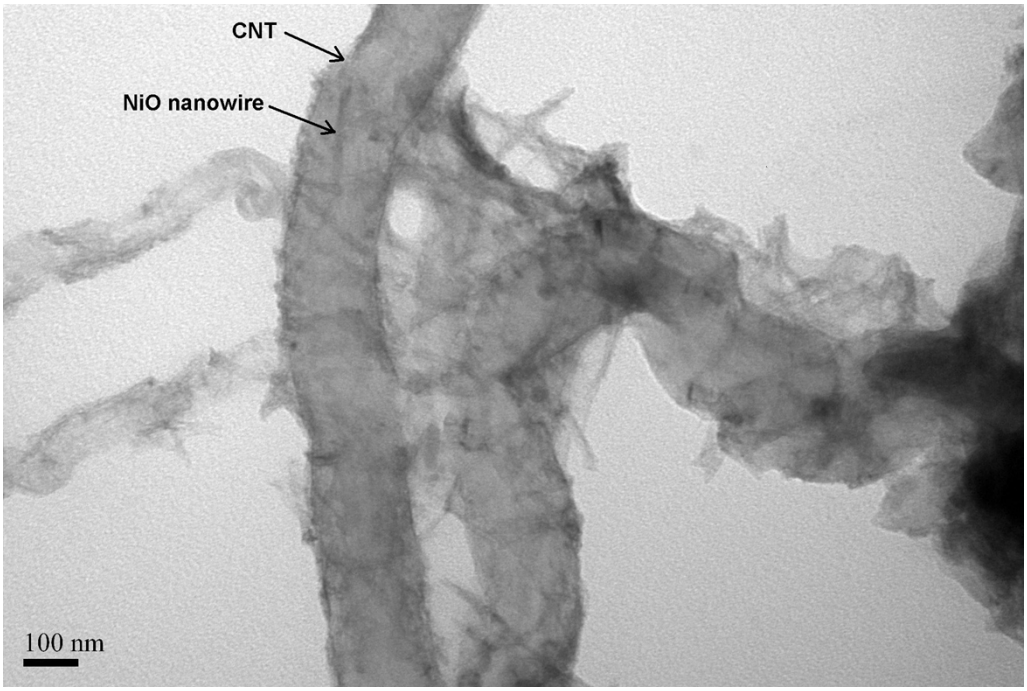

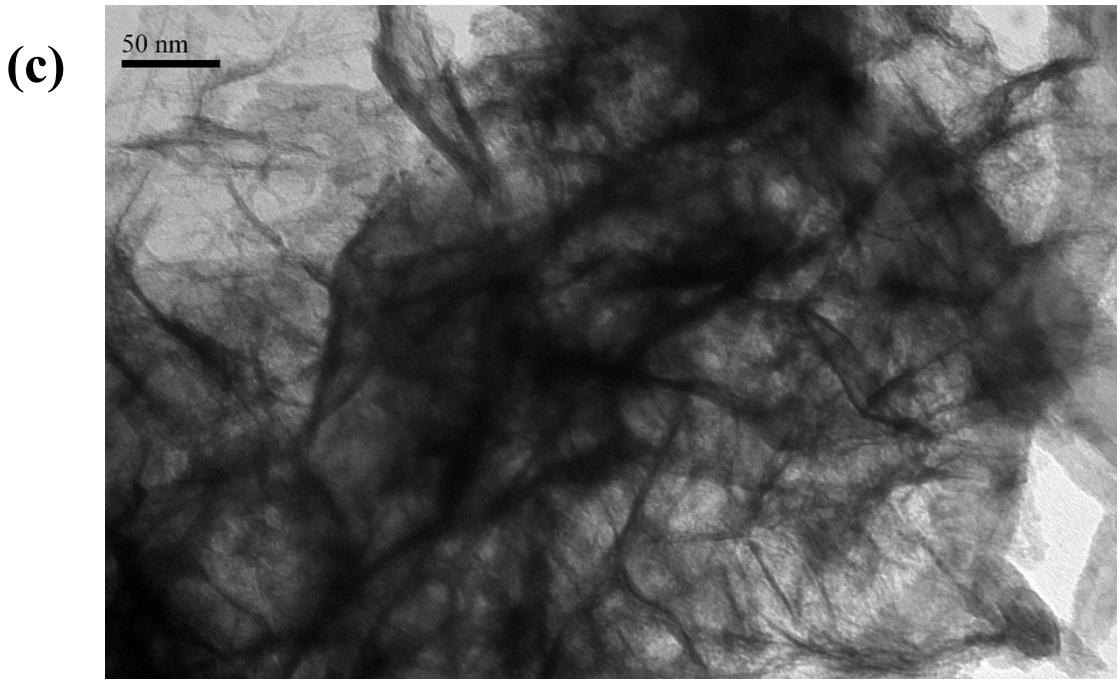

Fig. S2 TEM images of (a) NiO nanonet and (b,c) CNT film with attached NiO nanonet.

Thermal gravimetric analysis and X-ray diffraction patterns

TGA curve of the as-prepared nickel hydroxide sample is shown in Fig. S3. The weight loss from room temperature to 250°C results from the loss of surface and intercalated water (about 9 wt%). A sharp weight loss at the temperature range of 250-350°C comes from the decomposition of intercalated anions (SO_4^{2-}) and dehydroxylation of the brucite-like sheets, leading to the formation of nickel oxide.[1] Annealing temperature has been demonstrated to conspicuously affect both the specific surface area and electrical conductivity of nickel hydroxide. The optimum temperature range was found to be approximately 300-400°C in terms of the formation of non-stoichiometric nickel oxide which possesses both high electrical conductivity and large specific surface area.[2,3] When heated above 400°C, the nickel oxide (n-type semiconductor) has low electrical conductivity and poor electrochemical activity.[4] To achieve better electrochemical performance, the heating temperature of nickel hydroxide samples is therefore set at 300°C in this work.

Fig. S4a displays the XRD patterns of nickel hydroxide sample before and after

annealing at 300°C for 3 h. The nickel hydroxide grown on SS substrate can be characterized as α-$Ni(OH)_2$ (JCPDS No. 38-0715). During hydrothermal synthesis, OH^- ions generated from the hydrolysis of urea react with Ni^{2+} ions to form nickel hydroxide. The nascent nickel hydroxide nuclei experience a rapid adsorption and aggregation on surface of SS substrate. SO_4^{2-} anions and water molecules may intercalate into the interlayer space of the $Ni(OH)_2$ layers, leading to the formation of α-$Ni(OH)_2$.[5,6] The metastable α-$Ni(OH)_2$ can be converted to stable β-$Ni(OH)_2$ in the strong alkaline electrolyte. After annealing at 300°C, the diffraction peaks of nickel oxide appear. These peaks can be characterized as the cubic NiO (JCPDS No. 47-1049). Broad diffraction peaks of NiO are attributed to the poor crystallinity and small grain size, suggesting that the NiO can offer a large surface area to store charge. Fig. S4b shows the CNT and NiO/CNT films scraped from SS substrates. The CNT film shows a strong diffraction peak at $2\theta = 26.5°$, corresponding to the (002) peak for graphite (JCPDS, Card No. 75-1621). In NiO/CNT film, the diffraction peaks except for the diffraction peak of CNT can be characterized as cubic NiO similar to the NiO grown on SS substrate.

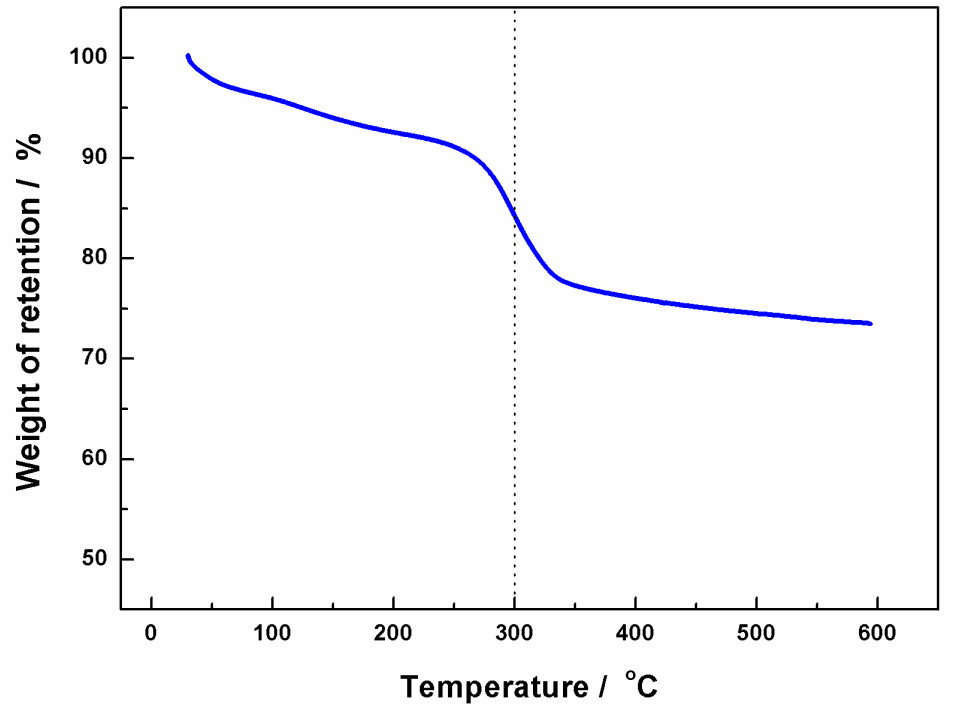

Fig. S3 TGA curve of the as-prepared nickel hydroxide sample.

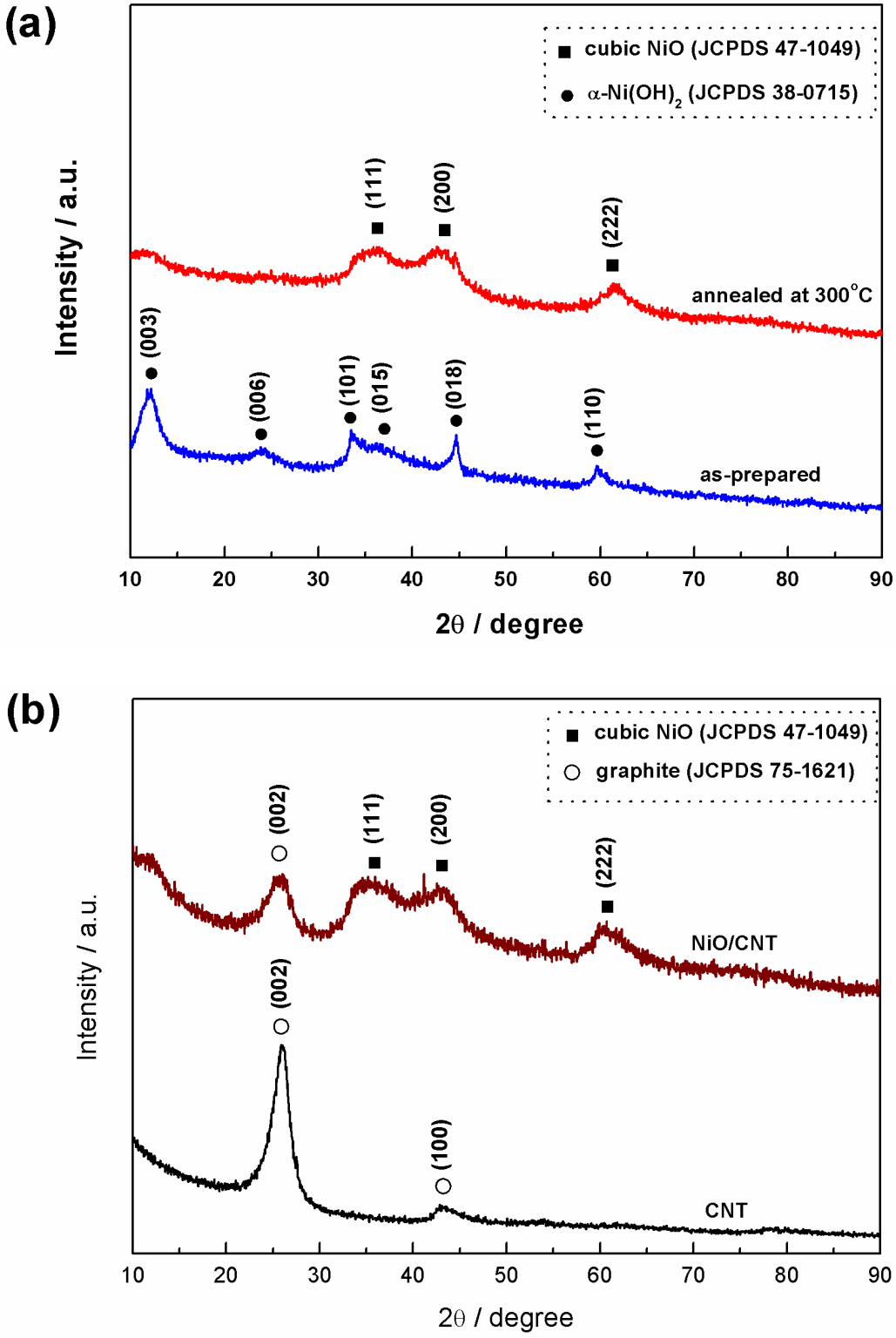

Fig. S4 (a) XRD patterns of the as-prepared and annealed nickel hydroxide samples. (b) XRD patterns of the CNT film and CNT film with attached NiO nanonet.

BET analysis of NiO and NiO/CNT samples

Fig. S5 shows nitrogen adsorption/desorption isotherms and pore size distribution of the NiO and NiO/CNT samples. Hysteresis between adsorption and desorption branch is observed, an indication of the existence of mesopores. The pore size distribution of the samples is given in the inset of Fig. S5. The majority of pores in NiO/CNT are located in the region of large mesopores (20-50 nm), while there are a number of small mesopores (< 10 nm) in the NiO sample. The BET surface area values for CNT, NiO, and NiO/CNT films were measured to be 54, 229 and 236 m^2 g^{-1}, respectively. Assuming proportional contributions from the NiO (63 wt%) and CNT (37 wt%) to the specific surface area of NiO/CNT, the specific surface area of NiO nanonet in the NiO/CNT composite can be evaluated to be approximately 343 m^{-2} g^{-1}. The increased surface area may result from the well dispersed NiO nanowires in the porous CNT networks.

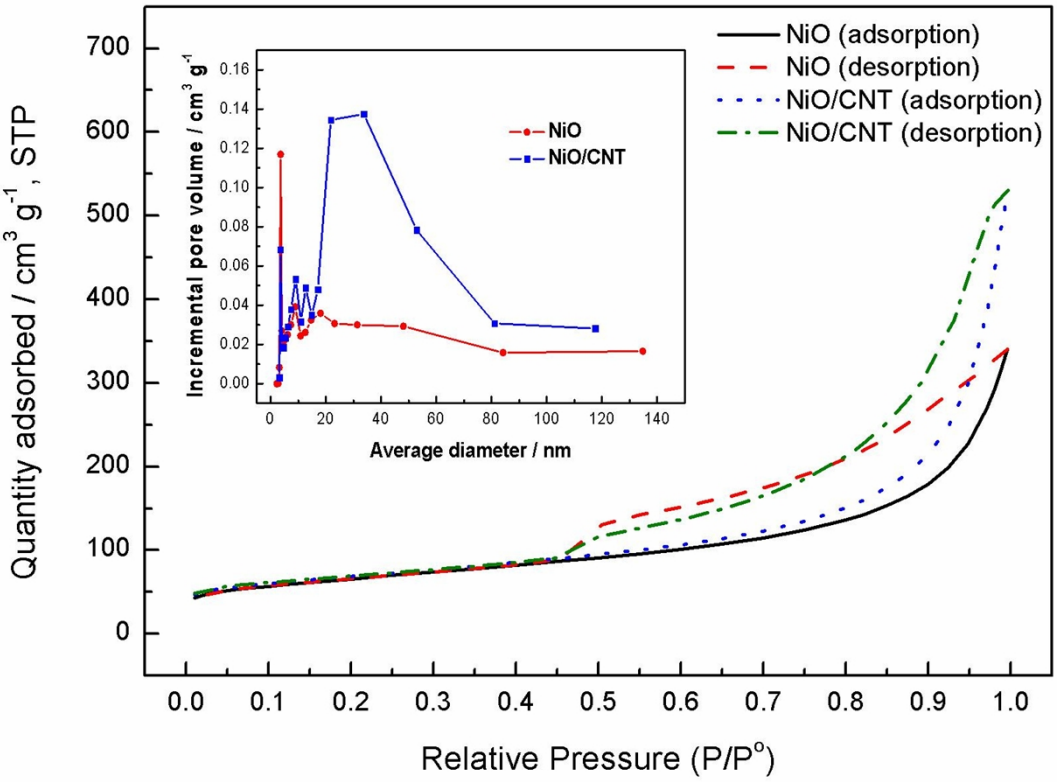

Fig. S5 Nitrogen adsorption/desorption isotherms of NiO and NiO/CNT samples. The inset shows the pore size distribution of the samples.

Electrochemical properties

Fig. S6a shows the galvanostatic charge/discharge curves of NiO/SS (SS-supported NiO nanonet) and NiO/CNT (CNT-supported NiO nanonet) electrodes at a current density of 30 A g^{-1}. The potential profile of NiO electrodes significantly differs from that of electric double-layer capacitors which exhibit a linear potential profile. A sloping potential profile with potential plateaus is observed in the NiO electrodes. The potential plateaus arise from the faradaic reaction between NiO and NiOOH. The discharging time of NiO/CNT electrode is considerably extended compared to that of NiO/SS electrode at a current density of 30 A g^{-1}. This result reflects that NiO/CNT electrode could provide much more active sites for faradaic reaction to occur, leading to an increase in the specific capacitance. The specific capacitance of electrodes during galvanostatic test can be calculated by the following equation:

$$C = i \cdot \Delta t / \Delta V \quad (1)$$

where C is the specific capacitance of electrode (F g^{-1}). ΔV is the potential window (V), and i is the charge or discharge current density (A g^{-1}), Δt is the charge or discharge time (s). The specific capacitance of NiO/CNT electrode discharged at 30 A g^{-1} could reach as high as 1536 F g^{-1}, which is much higher than that of NiO/SS electrode (995 F g^{-1}). The charging time and discharging time for each electrode are almost the same at a current density of 30 A g^{-1}, implying a high reversibility of the faradaic reaction on the NiO surface. The discharging curves of NiO/SS and NiO/CNT electrodes at various current densities are shown in Fig. S6b. The specific capacitance of NiO/CNT electrode decreases slightly with increasing the current density, while that of NiO/SS decreases significantly with increasing the current density. In addition, the NiO/CNT also shows a stable cycle-life performance (Fig. S7). The capacitance retention of NiO/CNT electrode remains 78 % after 5000 galvanostatic charge and discharge cycles at 50 A g^{-1}.

Fig. S8 shows the Nyquist plots of NiO electrodes at fully discharged state. An equivalent circuit used to fitting the Nyquist plots is shown in the inset of Fig. S8. The fitting values for the circuit elements using ZView software are tabulated in Table S1. The fitting results coincide with the experimental results. At very high frequencies, the intercept at the Z'-axis is a combinational ohmic resistance (R_s) resulting from the electrolyte, current collector, and active material/current collector interface. R_s of

NiO/CNT electrode (1.1 Ω) is lower than that of NiO/SS electrode (1.3 Ω), resulting from the introduction of conductive CNT networks to the NiO electrode. The semicircle in the high-frequency range corresponds to the charge-transfer resistance (R_{ct}) caused by the faradaic reaction and the double-layer capacitance (C_{dl}) on the NiO surface. R_{ct} of NiO/CNT electrode is approximately 1.3 Ω, which is much lower than that of NiO/SS electrode (4.2 Ω). An electrode with low R_{ct} is more effective for fast charge and discharge responses. At very low frequency, each electrode behaves like a pure capacitance, characterized by a vertical line parallel to the Z″-axis. A major difference is that the knee point shifts to more resistive value for the NiO/SS electrode. This is obviously attributed to the difference in the electrode structure, leading to a difference in the electrolyte penetration inside the porous structure of the NiO electrode. Clearly, the CNT-supported NiO nanonet electrode exhibits better porous structure for transport of electrolyte.

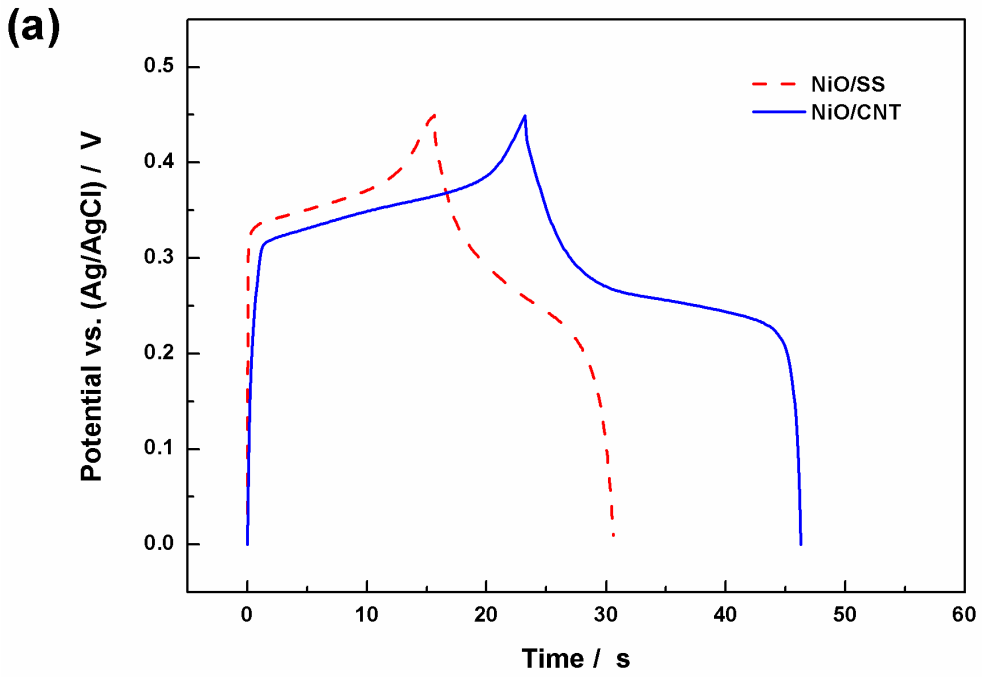

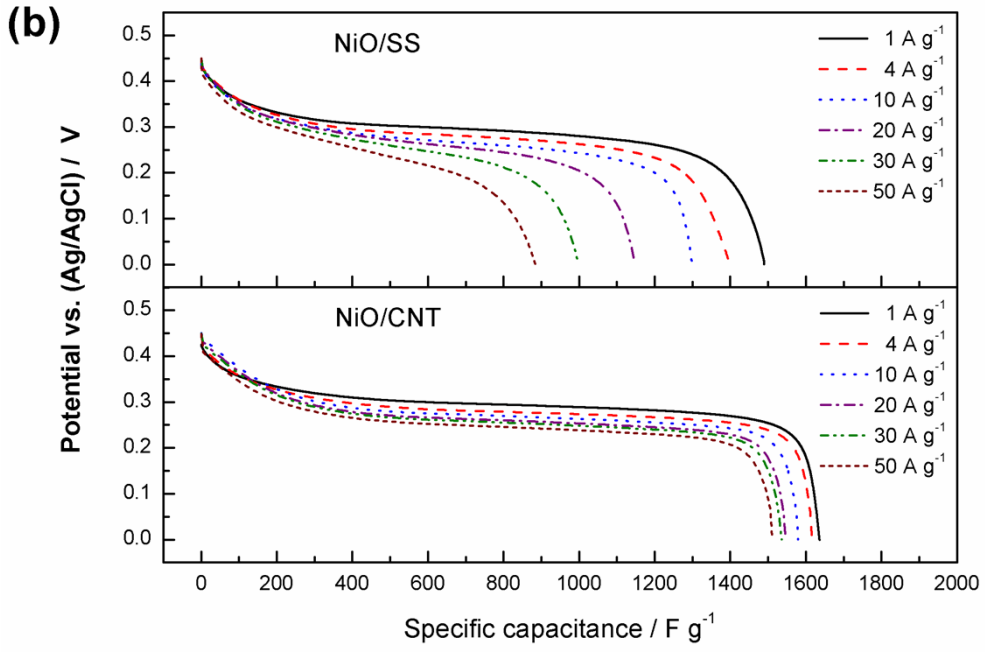

Fig. S6 (a) Galvanostatic charge/discharge curves of the NiO/SS and NiO/CNT electrodes at a current density of 30 A g^{-1}. (b) Discharging curves of NiO/SS and NiO/CNT electrodes at various current densities.

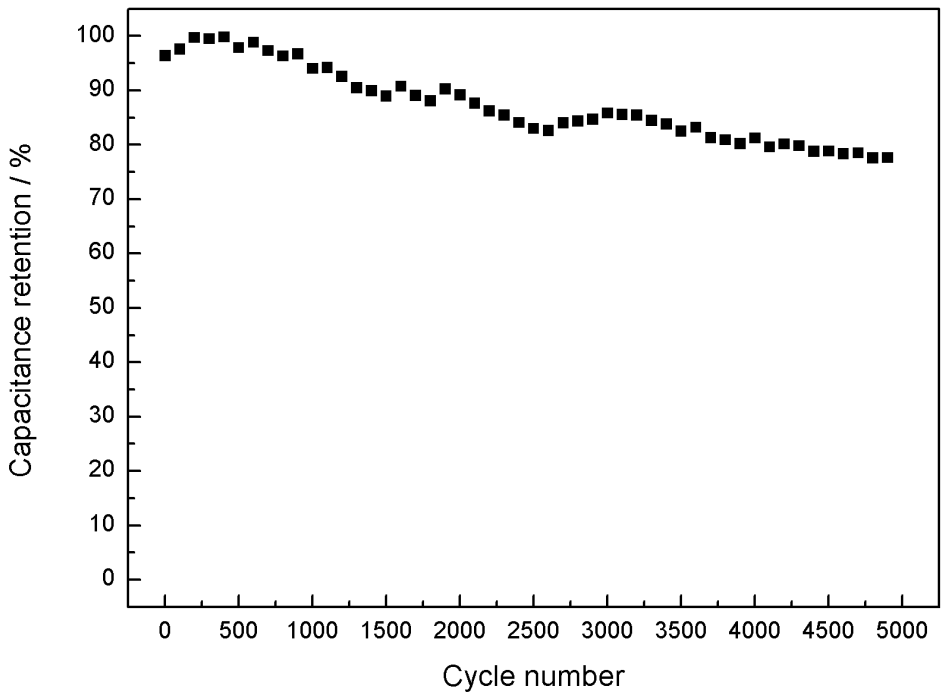

Fig. S7 Cycle-life stability of NiO/CNT electrode carried out at a charge/discharge current density of 50 A g^{-1}.

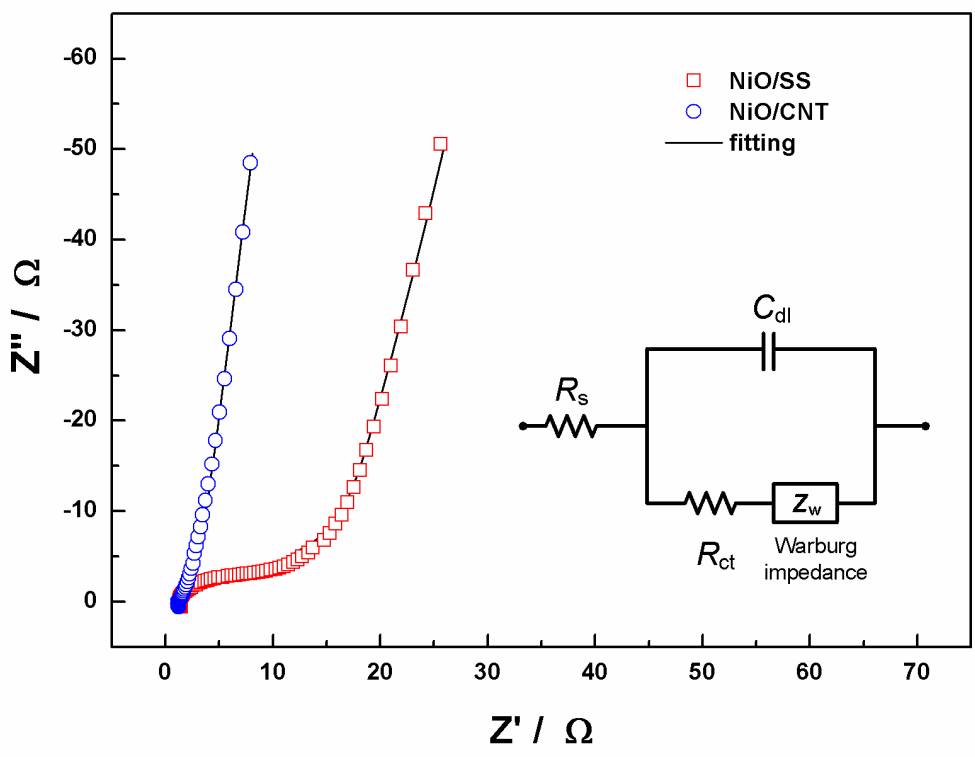

Fig. S8 Nyquist plots of the NiO/SS and NiO/CNT electrodes at a fully discharged state.

Table S1 Fitting results obtained from the electrochemical impedance spectra.

Electrode	R_s / Ω	C_{dl} / F	R_{ct} / Ω	Z_w		
				W-R/ Ω	W-T	W-P
NiO/SS	1.3	2.2×10^{-4}	4.2	31.4	0.77	0.44
	(4.2 %)	(5.2 %)	(2.3 %)	(2.0 %)	(2.6 %)	(0.5 %)
NiO/CNT	1.1	4.3×10^{-2}	1.3	0.9	0.02	0.46
	(4.0 %)	(10.6 %)	(11.1 %)	(6.4 %)	(8.4 %)	(0.7 %)

The error % is shown in the parenthesis.

References

1. M. Taibi, S. Ammar, N. Jouini, F. Fievet, P. Molinie and M. Drillon, *J. Mater. Chem.*, 2002, **12**, 3238-3244.
2. M.-S. Wu and H.-H. Hsieh, *Electrochim. Acta*, 2008, **53**, 3427-3435.
3. V. Srinivasan and J. W. Weidner, *J. Electrochem. Soc.*, 2000, **147**, 880-885.
4. C. H. Comniellis and I. A. Groza, *Thermochim. Acta*, 1988, **136**, 19-22.
5. L. Dong, Y. Chu and W. Sun, *Chem. Eur. J.*, 2008, **14**, 5064-5072.
6. L. Xu, Y.-S. Ding, C.-H. Chen, L. Zhao, C. Rimkus, R. Joesten and S. L. Suib, *Chem. Mater.*, 2007, **20**, 308-316.